Chapter 5
Numerical Solution of the Fokker–Planck Equation by Finite Difference and Finite Element Methods—A Comparative Study

L. Pichler, A. Masud, and L.A. Bergman

Abstract Finite element and finite difference methods have been widely used, among other methods, to numerically solve the Fokker–Planck equation for investigating the time history of the probability density function of linear and nonlinear 2d and 3d problems; also the application to 4d problems has been addressed. However, due to the enormous increase in computational costs, different strategies are required for efficient application to problems of dimension ≥ 3. Recently, a stabilized multi-scale finite element method has been effectively applied to the Fokker–Planck equation. Also, the alternating directions implicit method shows good performance in terms of efficiency and accuracy. In this paper various finite difference and finite element methods are discussed, and the results are compared using various numerical examples.

1 Introduction

The response of linear systems subjected to additive Gaussian white noise or linearly filtered Gaussian white noise is Gaussian. The derivation for an N-dimensional system can be found, e.g. in [11]. For the case of nonlinear systems subjected to additive Gaussian white noise, analytical solutions are restricted to certain scalar systems. It has been shown (see [2]), that the response of a multi-dimensional memoryless nonlinear system subjected to additive Gaussian white noise forms a vector Markov process, with transition probability density function satisfying both the forward (Fokker–Planck) and backward Kolmogorov equations for which numerical

L. Pichler · L.A. Bergman (✉)
Department of Aerospace Engineering, University of Illinois at Urbana-Champaign, 104 S. Wright Street, Urbana, IL 61801, USA
e-mail: lbergman@illinois.edu

L. Pichler
e-mail: Lukas.Pichler@ymail.com

A. Masud
Department of Civil and Environmental Engineering, University of Illinois at Urbana-Champaign, 205 N. Mathews Avenue, Urbana, IL 61801, USA
e-mail: amasud@illinois.edu

M. Papadrakakis et al. (eds.), *Computational Methods in Stochastic Dynamics*, Computational Methods in Applied Sciences 26,
DOI 10.1007/978-94-007-5134-7_5,

approximations in terms of finite element and finite difference methods can be pursued.

1.1 Scope of This Work

A number of numerical methods have been introduced over the past five decades to obtain approximate results for the solution of the Fokker–Planck equation (FPE). Many of these approximations can be shown to be accurate. This work deals with a review of several finite element and finite difference methods. A comparison and assessment of different methods is carried out by means of various numerical examples including a 2d linear, 2d unimodal and bimodal Duffing oscillators, 3d linear and 3d Duffing oscillators.

The goal is to evaluate the transient solution for the probability density function (PDF) of the oscillator due to stochastic (white noise) excitation. Thus, the forward Kolmogorov or Fokker–Planck equation is of interest and will be approximated within the numerical methods.

1.2 Background

The finite element method was first applied by [1] to determine the reliability of the linear, single degree-of-freedom oscillator subjected to stationary Gaussian white noise. The initial-boundary value problem associated with the backward Kolmogorov equation was solved numerically using a Petrov–Galerkin finite element method.

Reference [10] solved the stationary form of the FPE adopting the finite element method (FEM) to calculate the stationary probability density function of response. The weighted residual statement for the Fokker–Planck equation was first integrated by parts to yield the weak form of the equation.

The transient form of the FPE was analyzed in [16] using a Bubnov–Galerkin FEM. It was shown that the initial-boundary value problem can be modified to evaluate the first passage problem. A comparison for the reliability was carried out with the results obtained from the backward Kolmogorov equation.

A drawback of the FEM is the quickly increasing computational cost with increasing dimension. Thus, while 2 and 3 dimensional systems have been analyzed in the literature, the analysis of 4d or 5d problems reaches the limits of today's computational capabilities and are not yet feasible.

Computationally more economical—in terms of memory requirements, and when considering the effort spent for the assembly of the mass and stiffness matrices—are finite difference methods. The application of central differences is, as expected, only feasible for the case of 2d linear systems because of stability issues. The stability is a function of the nonlinearity and the dimension (ratio Δt and $\prod_{i=1}^{n} \Delta x_i$), thus being unfavorable for the use of this simple method.

A successful approach to overcome the limitations of simple finite differences was achieved by [20] in terms of higher order finite differences. The solution of a 4d system using higher order finite differences is reported in [20]. A comparison of various higher order FD formulations is presented in [9].

A viable approach to achieve higher accuracy is the application of operator splitting methods. Their capabilities with respect to the numerical solution of the FPE has so far received little attention. Operator splitting methods provide a tool to reduce the computational costs by the reduction of the solution to a series of problems of dimension one order less than the original problem. Thus, more efficiency, required for the solution of problems of larger dimension ($\geq$3), can be achieved. An operator splitting method for the solution of the 2d Duffing oscillator is presented in [23]. An operator splitting scheme for 3d oscillators subjected to additive and multiplicative white noise is given by [22]. The method consists of a series of consecutive difference equations for the three fluxes and is numerically stable. The alternating directions implicit method (ADI) [15] is adopted in this paper for a series of problems, and acceptably accurate results are achieved at low cost. The implementation of the method is straightforward and can be readily extended to higher dimensions.

Recent work by Masud et al. introduced a stabilized multi-scale finite element method which allows for a reduction of the number of elements for given accuracy and, thus, the efficiency of the computation can be increased by an order of magnitude when solving a 3d problem.

Several four-state dynamical systems were studied in [17, 18] in which the Fokker–Planck equation was solved using a global weighted residual method and extended orthogonal functions.

Meshless methods were proposed in [6, 7] to solve the transient FPE and [8] for the stationary FPE. Considerable reduction of the memory storage requirements is expected due to coarse meshes employed, and thus a standard desktop PC suffices to carry out the numerical analysis.

In addition, many numerical packages now provide the capability to solve partial differential equations by means of finite element and finite difference methods. However, in most cases these tools are limited to 2d and can only solve special forms of elliptic, parabolic or hyperbolic partial differential equations (PDE). The implementation of FD and FEM into computational software is shown for the cases of COMSOL (2d linear) and FEAP (general 3d).

2 The Fokker–Planck Equation

The Fokker–Planck equation for a n-dimensional system subjected to external Gaussian white noise excitation is given by

$$\frac{\partial p}{\partial t} = -\sum_{j=1}^{n} \frac{\partial}{\partial x_j}(z_j p) + \frac{1}{2}\left(\sum_{i=1}^{n}\sum_{j=1}^{n} \frac{\partial^2}{\partial x_i \, \partial x_j}(H_{ij} p)\right) \tag{5.1}$$

where p denotes the transition probability density function, $\mathbf{x}$ the n-dimensional state space vector and $\mathbf{z}(\mathbf{x})$ and $\mathbf{H}(\mathbf{x})$ denote the drift vector and diffusion matrix, respectively.

The normalization condition for the probability density function is given by

$$\int p_X(\mathbf{x}, t)\, d\mathbf{x} = 1, \tag{5.2}$$

and the initial conditions are given by $p_X(\mathbf{x}_0, 0)$. Examples for initial conditions are, e.g., deterministic, given by the Dirac delta function

$$p_X(\mathbf{x}_0, 0) = \prod_{i=1}^{n} \delta\big((x_i - x_{0i})\big) \tag{5.3}$$

and the n-dimensional Gaussian distribution

$$p_X(\mathbf{x}_0, 0) = \frac{1}{(2\pi)^{n/2} |\boldsymbol{\Sigma}|^{1/2}} \exp\left(-\frac{1}{2}(\mathbf{x} - \boldsymbol{\mu})^T \boldsymbol{\Sigma}^{-1} (\mathbf{x} - \boldsymbol{\mu})\right) \tag{5.4}$$

in the random case.

At infinity, a zero-flux condition is imposed

$$p(x_i, t) \to 0 \quad \text{as } x_i \to \pm\infty, i = 1, 2, \ldots, n \tag{5.5}$$

Without loss of generality, and for a better comparison, the various methods introduced will be examined for the 2d linear case,

$$\begin{Bmatrix} \dot{x_1} \\ \dot{x_2} \end{Bmatrix} = \begin{bmatrix} x_2 \\ -2\xi\omega x_2 - \omega^2 x_1 \end{bmatrix} + \begin{bmatrix} 0 \\ 1 \end{bmatrix} w(t) \tag{5.6}$$

The corresponding FPE is

$$\frac{\partial p}{\partial t} = -\frac{\partial (x_2 p)}{\partial x_1} + \frac{\partial [(2\xi\omega x_2 + x_1) p]}{\partial x_2} + D\frac{\partial^2 p}{\partial x_2^2} \tag{5.7}$$

which, after application of the chain rule, becomes

$$\frac{\partial p}{\partial t} = -x_2 \frac{\partial p}{\partial x_1} + (2\xi\omega x_2 + x_1)\frac{\partial p}{\partial x_2} + 2\xi\omega p + D\frac{\partial^2 p}{\partial x_2^2} \tag{5.8}$$

3 Finite Difference and Finite Element Methods

Many references deal with the application of FE and FD methods to the numerical solution of the Fokker–Planck equation (see e.g. [9, 19]).

3.1 Central Finite Differences

In terms of central finite differences, Eq. (5.8) becomes

$$\begin{aligned}\frac{p_{i,j}^{m+1}-p_{i,j}^{m}}{\Delta t} = &-x_2\frac{p_{i+1,j}^{m}-p_{i-1,j}^{m}}{2\Delta x_1}\\ &+2\xi\omega p_{i,j}^{m}+(2\xi\omega x_2)\frac{p_{i,j+1}^{m}-p_{i,j-1}^{m}}{2\Delta x_2}\\ &+D\frac{p_{i,j+1}^{m}-2p_{i,j}^{m}+p_{i,j-1}^{m}}{\Delta x_2^2}\end{aligned} \tag{5.9}$$

and an explicit formulation is obtained for the probability density function

$$\begin{aligned}p_{i,j}^{m+1} = p_{i,j}^{m}+\Delta t\Bigg(&-x_2\frac{p_{i+1,j}^{m}-p_{i-1,j}^{m}}{2\Delta x_1}\\ &+2\xi\omega p_{i,j}^{m}+(2\xi\omega x_2)\frac{p_{i,j+1}^{m}-p_{i,j-1}^{m}}{2\Delta x_2}\\ &+D\frac{p_{i,j+1}^{m}-2p_{i,j}^{m}+p_{i,j-1}^{m}}{\Delta x_2^2}\Bigg)\end{aligned} \tag{5.10}$$

The boundary conditions are given by $p_{i,j}=0$ for $i,\,j=1,N$. The discretization using central finite differences leads to an explicit scheme, which means that the values $p_{i,j}^{m+1}$ can be calculated directly from values $p_{i,j}^{m}$. Thus, the linear system of equations can be solved directly, and no inversion of the matrix relating $p_{i,j}^{m}$ to $p_{i,j}^{m+1}$ is required.

Explicit finite differences represent the simplest approximation; however, due to stability issues, implicit FD formulations are generally required.

Implicit, higher order finite difference schemes to solve Fokker–Planck equations have been developed by [20]. Higher order FD lead to more accurate results, but they are not used for comparison herein.

3.2 Alternating Directions Implicit Method

The alternating directions implicit method (ADI) is a finite difference scheme, for which the finite difference steps in each direction are resolved separately and in each step implicitly for one dimension and explicitly for the others, leading to a stable formulation. The main advantages are that the resulting operational matrix is tridiagonal and, thus, its inverse can be computed efficiently. Moreover, the dimensionality of the problem is reduced by one, and the problem is reduced to the solution of a series of problems of dimension of one order lower.

In Eq. (5.8), finite differences are first applied implicitly to the x_1-direction

$$\frac{p_{i,j}^{m+1/2} - p_{i,j}^{m}}{\Delta(t/2)} = -x_2 \frac{p_{i+1,j}^{m+1/2} - p_{i-1,j}^{m+1/2}}{2\Delta x_1} + 2\xi\omega p_{i,j}^{m} + (2\xi\omega x_2) \frac{p_{i,j+1}^{m} - p_{i,j-1}^{m}}{2\Delta x_2} + D \frac{p_{i,j+1}^{m} - 2p_{i,j}^{m} + p_{i,j-1}^{m}}{\Delta x_2^2} \tag{5.11}$$

and then to the x_2-direction.

$$\frac{p_{i,j}^{m+1} - p_{i,j}^{m+1/2}}{\Delta(t/2)} = -x_2 \frac{p_{i+1,j}^{m+1/2} - p_{i-1,j}^{m+1/2}}{2\Delta x_1} + 2\xi\omega p_{i,j}^{m+1/2} + (2\xi\omega x_2) \frac{p_{i,j+1}^{m+1} - p_{i,j-1}^{m+1}}{2\Delta x_2} + D \frac{p_{i,j+1}^{m+1} - 2p_{i,j}^{m+1} + p_{i,j-1}^{m+1}}{\Delta x_2^2} \tag{5.12}$$

Both Eq. (5.11) and Eq. (5.12) give $M-2$ tridiagonal linear systems of equations in x_1 for the $j = 2, \ldots, M-1$ values of x_2, and in case of Eq. (5.11) $M-2$ tridiagonal linear systems of equations in x_2 for the $i = 2, \ldots, M-1$ values of x_1.

The computational cost is mainly due to the n times N matrix inversions which are encountered in the n-loops solution for a full time step; n denotes the dimension of the problem and N the number of nodes per dimension.

3.3 Finite Element Method

Reduction of Eq. (5.1) to the weak form and the introduction of shape functions of C^0 continuity lead to

$$\mathbf{C}\dot{p} + Kp = 0 \tag{5.13}$$

where

$$C_{rs}^{e} = \int_{\Omega^e} N_r(\mathbf{x}) N_s(\mathbf{x})\, d\mathbf{x} \tag{5.14}$$

and

$$K_{rs}^{e} = \int_{\Omega^e} \left(\sum_{i=1}^{n} z_i(\mathbf{x}) N_s \frac{\partial}{\partial x_i} N_r\, d\mathbf{x} - \sum_{i=1}^{n} \sum_{j=1}^{n} \frac{\partial}{\partial x_i} N_r \frac{\partial}{\partial x_i} [H_{ij} N_s]\, d\mathbf{x} \right) \times N_r(\mathbf{x}) N_s(\mathbf{x})\, d\mathbf{x} \tag{5.15}$$

The integration over time can be performed in a suitable way using the Crank–Nicholson scheme ($\theta = 0.5$).

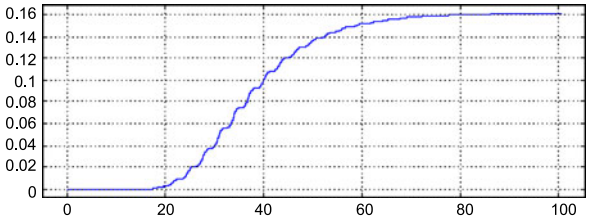

Fig. 5.1 Probability density function $p(0, 0, t)$ at central node over time

3.4 Multi-scale Finite Element Method

The multi-scale FEM used herein was introduced by [14] for the numerical treatment of advection-diffusion equations in fluid dynamics. Then, the methodology was extended by [13] to the special case of the Fokker–Planck equation. Finally, the method was applied to the numerical solution of the Fokker–Planck equation of a 3d linear system [12]; [5] provide an overview of stabilized finite element methods and recent developments of their application to the advection-diffusion equation.

For a description of the method the reader is referred to the aforementioned references. Basically, a multi-scale FEM means that an approximation of the error term from the traditional FE formulation is included at a fine scale into the formulation; the probability density function is then given by

$$p = \hat{p} + p' \tag{5.16}$$

where $\hat{p}$ represents the contribution of the coarse scale and p' the contribution of the fine scale.

3.5 Implementation Within COMSOL/FEAP

The FE code COMSOL provides the possibility to solve partial differential equations by finite differences. For an extensive discussion, refer to the COMSOL documentation [4]. Figure 5.1 shows the results obtained for the FPE for the 2d linear oscillator with parameters to be discussed later.

The multiscale finite element method was implemented by Masud and coworkers into the finite element code FEAP and is used herein for comparison of the 3d examples.

4 Numerical Examples

The numerical methods used in this comparison are:

1. central finite differences (FD)
2. alternating directions implicit method (ADI)

Table 5.1 Parameter for the linear oscillator

μ	σ	ξ	ω	D
$[5, 5]$	$\frac{1}{9}\mathbf{I}(2)$	0.05	1	0.1

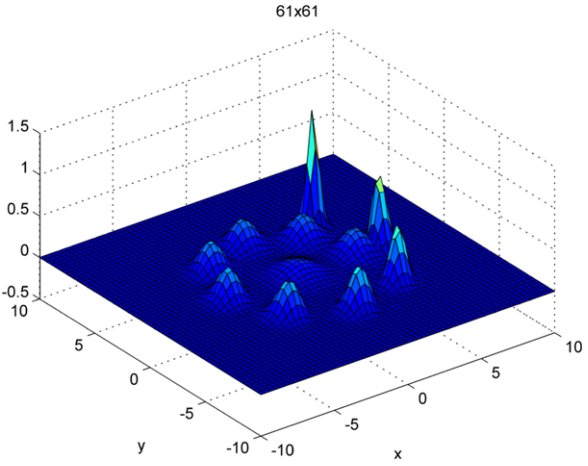

Fig. 5.2 FEM: 61×61—Probability density function $p(t)$ over time

3. Bubnov–Galerkin finite element method (FEM)
4. stabilized multiscale finite element method (MSFEM)

The methods 1–3 are coded in MATLAB and the analysis was carried out on a 64-bit Windows server (32 GB). The results for method 4 are obtained on 32 bit Linux or Windows machines with 2 GB memory using an implementation within FEAP [13].

4.1 2-d Linear Oscillator

The different methods are applied to solve the FPE for the linear oscillator (see Eq. (5.6)). The parameters of the oscillator are chosen according to [16] and are described in Table 5.1, were $\mathbf{I}(2)$ denotes the identity matrix in 2-d:

Finite element results obtained using a 61×61 mesh are shown in Fig. 5.2 and Fig. 5.3. All results are calculated with a time increment of $\Delta t = 0.001$ and a total time of $\tau = 20$ natural periods. The state space is discretized on the domain $[-10, 10] \times [-10, 10]$;

Figure 5.2 shows the evolution of the probability density function over time. In Fig. 5.3 the transient solution for the PDF at the origin is given. The exact stationary value at the origin is $p_{stat}(0, 0) = 1.5915e - 1$.

The accuracy of the numerical solutions are compared at stationarity (i.e., after $t = 20$ cycles) using two error measures. The first, the maximum norm

$$\|e\|_\infty = \left\| p^{ex} - p^{num} \right\|_\infty \tag{5.17}$$

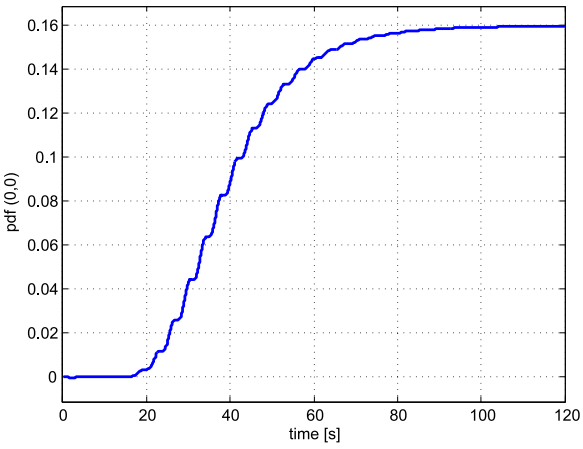

Fig. 5.3 FEM: 61×61—Probability density function at central node $p(0, 0, t)$ over time

is a measure of the maximum error across the entire mesh. The second, the Euclidean norm

$$\|e\|_2 = \left\| p^{ex} - p^{num} \right\|_2 \tag{5.18}$$

can be used to describe the average nodal error $\overline{e} = \|e\|_2 / n_{nodes}$, where n_{nodes} is the total number of nodes.

Table 5.2 correctly visualizes the increasing accuracy for all methods when the mesh is refined. It can also be seen that the FD and ADI deliver similar results. The advantage of the ADI over FD is that the stability of the method allows one to use larger time steps. The FEM provides more accurate results for the same mesh refinement as the finite difference methods. The FEM is the preferable method to investigate the first passage problem in case small probabilities of failure are involved and a highly accurate method is required.

Alternatively, the accuracy of the solution at stationarity can also be represented by comparison of the exact and numerical covariance matrices K_{xx}, the latter computed from FE/FD results for the PDF.

The transient solution for the probability density at the center node can be obtained with all three methods as listed in Table 5.2. Figure 5.4 shows a comparison for the PDF at the origin using finite difference method and different mesh sizes.

Table 5.2 Comparison of the accuracy for the linear oscillator

Method/Mesh	61×61		81×81		101×101		121×121	
	$\|e\|_\infty$	$\|e\|_2$	$\|e\|_\infty$	$\|e\|_2$	$\|e\|_\infty$	$\|e\|_2$	$\|e\|_\infty$	$\|e\|_2$
FD	7.05e-3	2.99e-2	4.169e-3	2.405e-2	2.983e-3	2.201e-2	2.371e-3	2.199e-2
ADI	1.66e-2	4.61e-2	4.144e-3	2.375e-2	2.931e-3	2.149e-2	2.305e-3	2.124e-2
FEM	2.04e-3	1.00e-2	1.712e-3	1.152e-2	1.550e-3	1.370e-2	1.464e-3	1.613e-2

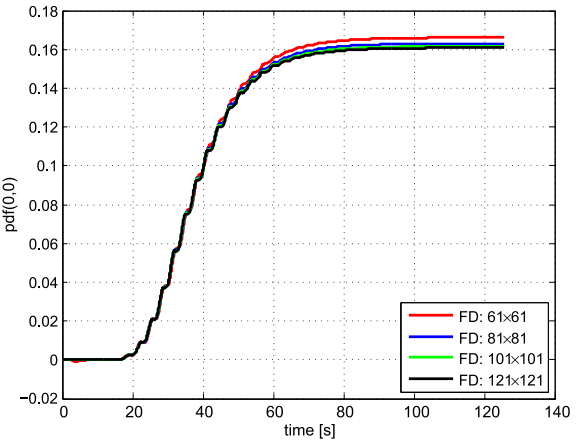

Fig. 5.4 FD—Comparison for probability density function at central node $p(0, 0, t)$ over time

Table 5.3 Parameters for the unimodal Duffing oscillator

μ	σ	ξ	ω	D	γ
$[0, 10]$	$\frac{1}{2}\mathbf{I}(2)$	0.2	1	0.4	0.1

4.2 2-d Duffing Oscillator

Both, the unimodal Duffing-oscillator and the bimodal Duffing-oscillator as well are investigated in the following.

4.2.1 Unimodal

The unimodal Duffing oscillator is considered next:

$$\begin{bmatrix} \dot{x_1} \\ \dot{x_2} \end{bmatrix} = \begin{bmatrix} x_2 \\ -2\xi\omega x_2 - \omega^2 x_1 - \omega^2 \gamma x_1^3 \end{bmatrix} + \begin{bmatrix} 0 \\ 1 \end{bmatrix} w(t) \tag{5.19}$$

The parameters of the oscillator are chosen as in Table 5.3.

The state space is discretized on the domain $[-15, 15] \times [-15, 15]$.

It is known that central finite differences are not suitable in case of nonlinearities, but ADI can be utilized nonetheless. When the Duffing-oscillator is analyzed, it is found that the ADI can be used due to its implicit formulation with the largest time step Δt, thus providing a good compromise between accuracy and efficiency as can be seen from Table 5.4. The time steps used are $\Delta t = 1e-2$ (ADI), $\Delta t = 1e-3$ (FEM) and $\Delta t = 5e-4$ (FEM: mesh 101).

Table 5.4 Comparison of the accuracy for the unimodal Duffing oscillator

Method/Mesh	61×61		81×81		101×101	
	$\|e\|_\infty$	$\|e\|_2$	$\|e\|_\infty$	$\|e\|_2$	$\|e\|_\infty$	$\|e\|_2$
ADI	1.7832e-2	4.9323e-2	9.6731e-3	3.5553e-2	6.1694e-3	2.8444e-2
FEM	2.6002e-3	1.1587e-2	1.3999e-3	8.5297e-3	9.3290e-4	6.8215e-3

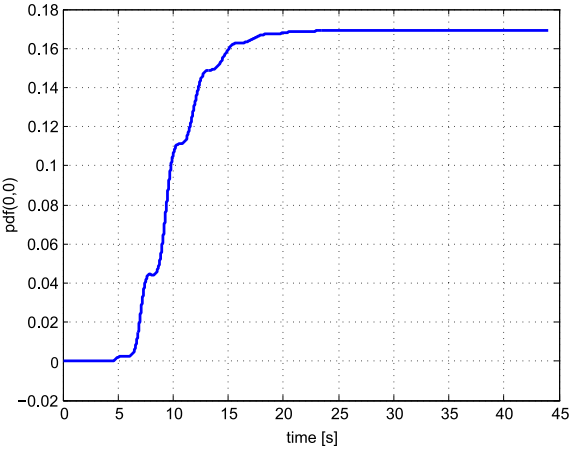

Fig. 5.5 FEM: 101×101—Probability density function at central node $p(0, 0, t)$ over time

The exact analytical expression for the stationary PDF of the unimodal Duffing oscillator of Eq. (5.19) is given by

$$\begin{aligned} \sigma_{x_0}^2 &= \frac{\pi G_0}{4\xi\omega_0^3} \\ \sigma_{v_0}^2 &= \omega_0^2 \sigma_{x_0}^2 \\ p_X(\mathbf{x}) &= C \exp\left(-\frac{1}{2\sigma_{x_0}^2}\left(x^2 + \frac{\gamma}{2}x^4\right) - \frac{1}{2}\sigma_{v_0}^2 v^2\right) \end{aligned} \tag{5.20}$$

The value of the stationary probability density function at the central node is $p_{stat}(0, 0) = 1.6851e - 1$. Figure 5.5 shows the evolution of the PDF at central node $p(0, 0, t)$ over time using the FEM and a mesh of 101×101.

4.2.2 Bimodal

The equations for the bimodal Duffing oscillator are characterized by the changed sign of the term $\omega^2 x_1$.

$$\begin{bmatrix} \dot{x_1} \\ \dot{x_2} \end{bmatrix} = \begin{bmatrix} x_2 \\ -2\xi\omega x_2 + \omega^2 x_1 - \omega^2 \gamma x_1^3 \end{bmatrix} + \begin{bmatrix} 0 \\ 1 \end{bmatrix} w(t) \tag{5.21}$$

Table 5.5 Parameter for the bimodal Duffing oscillator

μ	σ	ξ	ω	D	γ
$[0, 10]$	$\frac{1}{2}\mathbf{I}(2)$	0.2	1	0.4	0.1

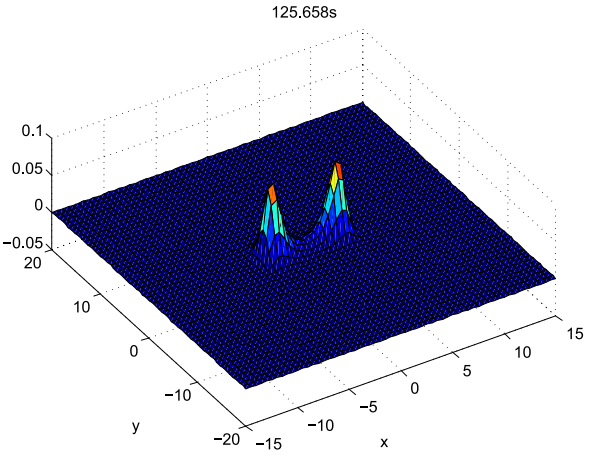

Fig. 5.6 61×61: Stationary probability density function p_{stat}

The parameters of the oscillator are chosen according to [16] and are given in Table 5.5.

The state space is discretized on the domain $[-15, 15] \times [-15, 15]$. Again, the ADI provides a tool for obtaining accurate results rather quickly.

In Fig. 5.6 the PDF is depicted for stationary conditions and a 61×61 mesh. A comparison of the evolution of the probability density function at the origin is shown in Fig. 5.7 for FEM and different meshes.

To compare the solution, the analytical expression according to [3] should be used. The exact analytical expression for the bimodal Duffing oscillator of Eq. (5.21) is given as

$$p_X(\mathbf{x}) = C \exp\left(-\frac{1}{2\sigma_{x_0}^2}\left(-x^2 + \frac{\gamma}{2}x^4\right) - \frac{1}{2}\sigma_{v_0}^2 v^2\right)$$

The value of the stationary PDF at the central node is $p_{stat}(0, 0) = 8.3161e - 3$. Table 5.6 shows a comparison of the accuracy for different mesh sizes for the bimodal Duffing oscillator. The maximum value of the stationary PDF of the bimodal oscillator at $x_{1,2} = \pm\sqrt{1/\gamma} = \pm 3.1623$ and $y_{1,2} = 0$ is $p_{stat}(x_{1,2}, 0) = 0.1013$. A comparison of the evolution of the probability density function at the mesh point $(x = 3,\ y = 0)$ which is closest to the maximum of the PDF is shown in Fig. 5.8 for FEM and different meshes; $p_{stat}(3, 0) = 0.0988$.

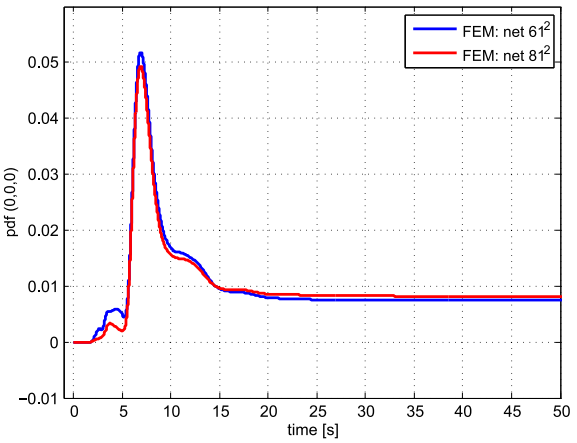

Fig. 5.7 FEM: Comparison of the probability density function at the central node $p(0,0,t)$ over time

4.3 3-d Linear Oscillator

A 3-rd state variable is introduced in terms of a low pass filter for the white noise excitation which is applied to the linear 2d system.

$$\begin{bmatrix} \dot{x_1} \\ \dot{x_2} \\ \dot{x_3} \end{bmatrix} = \begin{bmatrix} x_2 \\ -2\xi\omega x_2 - \omega^2 x_1 + x_3 \\ -\alpha x_3 \end{bmatrix} + \begin{bmatrix} 0 \\ 0 \\ 1 \end{bmatrix} w(t) \tag{5.22}$$

The parameters of the 3d linear oscillator are given in Table 5.7.

Tables 5.8 and 5.9 show a comparison of the accuracy of the results for the linear oscillator. The time step is chosen to be $\Delta t = 0.01$, and only for FEM (net 81^3) $\Delta t = 0.001$ is required. The exact stationary value of the PDF at the origin is $p_{stat}(0,0,0) = 0.2409$. Figure 5.9 shows a comparison for the evolution of the PDF at the central node. The exact analytical solution is compared with the ADI and the FEM using various mesh sizes.

Table 5.6 Comparison of the accuracy for the bimodal Duffing oscillator

Method/Mesh	61×61		81×81		101×101	
	$\|e\|_\infty$	$\|e\|_2$	$\|e\|_\infty$	$\|e\|_2$	$\|e\|_\infty$	$\|e\|_2$
ADI	4.7186e-2	1.8229e-1	1.1899e-2	4.2491e-2	7.5077e-3	3.0640e-2
FEM	6.8085e-3	1.9074e-2	2.6024e-3	1.1265e-2	2.8419e-3	1.3709e-2

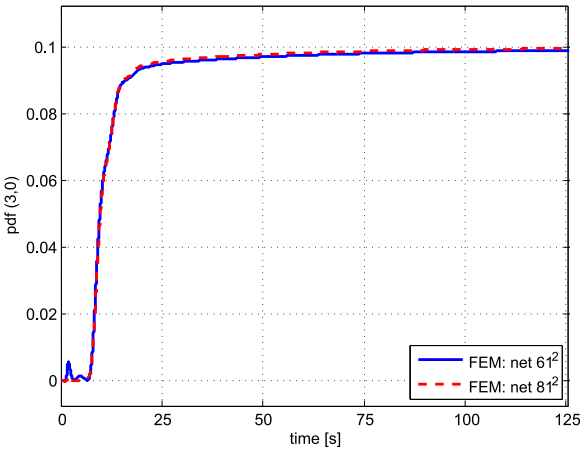

Fig. 5.8 FEM: Comparison of the probability density function at the node $p(3,0,t)$ over time

Table 5.7 Parameter for the 3d linear oscillator

μ	σ	ξ	ω	D	α
$[0,0,0]$	$0.2\mathbf{I}(3)$	0.2	1	0.4	1

4.4 3-d Duffing Oscillator

$$\begin{bmatrix} \dot{x_1} \\ \dot{x_2} \\ \dot{x_3} \end{bmatrix} = \begin{bmatrix} x_2 \\ -2\xi\omega x_2 - \omega^2 x_1 - \omega^2 \gamma x_1^3 + x_3 \\ -\alpha x_3 \end{bmatrix} + \begin{bmatrix} 0 \\ 0 \\ 1 \end{bmatrix} w(t) \tag{5.23}$$

The parameters of the 3d Duffing oscillator are given in Table 5.10.

Table 5.8 Comparison of the accuracy for the 3-d linear oscillator

Method/Mesh	25^3		41^3	
	$\|e\|_\infty$	$\|e\|_2$	$\|e\|_\infty$	$\|e\|_2$
ADI	1.8009e-1	3.6649e+0	4.8336e-2	4.8748e-1
FEM	6.5802e-3	4.6480e-2	3.5574e-3	4.6357e-2
MSFEM	1.2533e-2	5.0262e-2	—	—

Table 5.9 Comparison of the accuracy for the 3-d linear oscillator

Method/Mesh	61^3		81^3		101^3	
	$\|e\|_\infty$	$\|e\|_2$	$\|e\|_\infty$	$\|e\|_2$	$\|e\|_\infty$	$\|e\|_2$
ADI	1.2542e-2	2.1170e-1	6.9165e-3	1.8067e-1	4.3899e-3	1.6063e-1
FEM	1.4081e-3	3.4554e-2	3.9016e-4	2.4920e-2	—	—

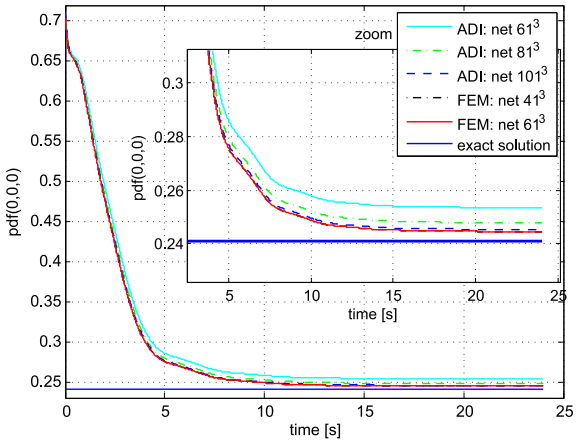

Fig. 5.9 Probability density function at the central node $p(0, 0, 0, t)$ over time

Table 5.10 Parameters for the 3d Duffing oscillator

μ	σ	ξ	ω	D	α	γ
$[0, 0, 0]$	$0.2\mathbf{I}(3)$	0.2	1	0.4	1	0.1

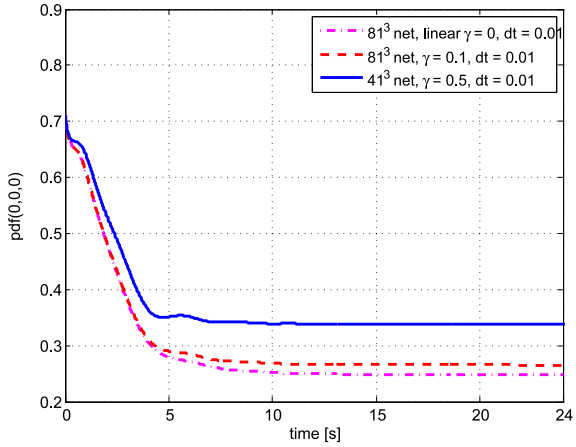

Fig. 5.10 Probability density function at the central node $p(0, 0, 0, t)$ over time

Figure 5.10 shows converged results for the evolution of the PDF at the origin over time using ADI for two different degrees of nonlinearity and for the corresponding linear system ($\gamma = 0$).

5 Discussion

Despite the greater numerical effort, the FEM is preferable over FD, because it yields more accurate results. However, at this time the FEM is only suitable for

dimension ≤ 3. In the case of 3d and 4d problems, the stabilized multi-scale FEM provides a tool with a high order of accuracy, preserving numerical efficiency due to the fact that a coarser mesh size can be used.

The first effective numerical solution for 4d problems was reported by [21] in terms of high-order finite differences. The advantage of operator splitting methods including the ADI is the stability of the method, meaning that larger time steps (when compared to FEM) can be used, thus speeding up the analysis as the dimensionality of the problem is reduced by one.

The recently introduced PUFEM (see Kumar et al.) represents a possibility to obtain good results with coarse mesh sizes. The price paid is the computational overhead required in order to allow for the proposed coarse mesh size.

From the above discussion it is clear that future developments will be bounded by the so-called curse of dimensionality for some time.

Acknowledgements This research was partially supported by the Austrian Research Council FWF under Project No. J2989-N22 (LP, Schrödinger scholarship).

References

1. Bergman, L.A., Heinrich, J.C.: On the reliability of the linear oscillator and systems of coupled oscillators. Int. J. Numer. Methods Eng. **18**(9), 1271–1295 (1982)
2. Caughey, T.K.: Derivation and application of the Fokker–Planck equation to discrete nonlinear dynamic systems subjected to white random excitation. J. Acoust. Soc. Am. **35**(11), 1683–1692 (1963)
3. Caughey, T.K.: Nonlinear Theory of Random Vibrations. Elsevier, Amsterdam (1971)
4. COMSOL 5.5: Theory manual. COMSOL (2011)
5. Franca, L.P., Hauke, G., Masud, A.: Revisiting stabilized finite element methods for the advective-diffusive equation. Comput. Methods Appl. Mech. Eng. **195**(13–16), 1560–1572 (2006)
6. Kumar, M., Chakravorty, S., Junkins, J.L.: A homotopic approach to domain determination and solution refinement for the stationary Fokker–Planck equation. Probab. Eng. Mech. **24**(3), 265–277 (2009)
7. Kumar, M., Chakravorty, S., Junkins, J.L.: A semianalytic meshless approach to the transient Fokker–Planck equation. Probab. Eng. Mech. **25**(3), 323–331 (2010)
8. Kumar, M., Chakravorty, S., Singla, P., Junkins, J.L.: The partition of unity finite element approach with hp-refinement for the stationary Fokker–Planck equation. J. Sound Vib. **327**(1–2), 144–162 (2009)
9. Kumar, P., Narayana, S.: Solution of Fokker–Planck equation by finite element and finite difference methods for nonlinear systems. Sâdhana **31**(4), 445–461 (2006)
10. Langley, R.S.: A finite element method for the statistics of non-linear random vibration. J. Sound Vib. **101**(1), 41–54 (1985)
11. Lin, Y.K.: Probabilistic Theory of Structural Dynamics. Krieger, Melbourne (1976)
12. Masud, A., Bergman, L.A.: Solution of the four dimensional Fokker–Planck equation: still a challenge. In: Augusti, G., Schuëller, G.I., Ciampoli, M. (eds.) ICOSSAR 2005. Millpress, Rotterdam (2005)
13. Masud, A., Bergman, L.A.: Application of multi-scale finite element methods to the solution of the Fokker–Planck equation. Comput. Methods Appl. Mech. Eng. **194**(12–16), 1513–1526 (2005)

14. Masud, A., Khurram, R.A.: A multiscale/stabilized finite element method for the advection-diffusion equation. Comput. Methods Appl. Mech. Eng. **193**(21–22), 1997–2018 (2004)
15. Peaceman, D.W., Rachford, H.H.: The numerical solution of parabolic and elliptic differential equations. J. Soc. Ind. Appl. Math. **3**, 28–41 (1955)
16. Spencer, B.F., Bergman, L.A.: On the numerical solutions of the Fokker–Planck equations for nonlinear stochastic systems. Nonlinear Dyn. **4**, 357–372 (1993)
17. von Wagner, U., Wedig, W.V.: On the calculation of stationary solutions of multi-dimensional Fokker–Planck equations by orthogonal functions. Nonlinear Dyn. **21**(3), 289–306 (2000)
18. Wedig, W.V., von Wagner, U.: Extended Laguerre polynomials for nonlinear stochastic systems. In: Computational Stochastic Mechanics. Balkema, Rotterdam (1999)
19. Wijker, J.: Random Vibrations in Spacecraft Structures Design: Theory and Applications. Solid Mechanics and Its Applications, vol. 165. Springer, Berlin (2009)
20. Wojtkiewicz, S.F., Bergman, L.A., Spencer, B.F.: High fidelity numerical solutions of the Fokker–Planck equation. In: Seventh International Conference on Structural Safety and Reliability (ICOSSAR'97) (1998)
21. Wojtkiewicz, S.F., Bergman, L.A., Spencer, B.F., Johnson, E.A.: Numerical solution of the four-dimensional nonstationary Fokker–Planck equation. In: Narayanan, S., Iyengar, R.N. (eds.) IUTAM Symposium on Nonlinearity and Stochastic Structural Dynamics (1999)
22. Xie, W.-X., Cai, L., Xu, W.: Numerical simulation for a Duffing oscillator driven by colored noise using nonstandard difference scheme. Physica A **373**, 183–190 (2007)
23. Zorzano, M., Mais, H., Vázquez, L.: Numerical solution of two dimensional Fokker–Planck equations. Appl. Math. Comput. **98**, 109–117 (1999)